

Spontaneous quantum Hall effect via thermally induced quadratic Fermi point

Gia-Wei Chern^{1,2} and C. D. Batista¹

¹*Theoretical Division, Los Alamos National Laboratory, Los Alamos, New Mexico 87545, USA*

²*Department of Physics, University of Wisconsin, Madison, Wisconsin 53706, USA*

(Dated: May 11, 2021)

Gapless electronic systems containing topologically nontrivial Fermi points are sources of various topological insulators. Whereas most of these special band-crossing points are built in the electronic structure of the non-interacting lattice models, we show that a quadratic Fermi point characterized by a non-zero winding number emerges with a collinear triple- \mathbf{Q} spin-density-wave state that arises from a perfectly nested but topologically trivial Fermi surface. We obtain a universal low-energy Hamiltonian for the quadratic Fermi point and show that such collinear orderings are unstable against the onset of scalar spin chirality that opens a gap and induces a spontaneous quantum Hall insulator as the temperature tends to zero.

Fermi points with nontrivial Berry connection have recently been the focus of intense theoretical and experimental effort. These singular points are the momentum-space counterpart of topological defects in ordered media; both are characterized by a topological invariant [1]. Topological Fermi points are usually robust against small perturbations which preserve certain discrete symmetries of the system. On the other hand, when a gap opens at a singular Fermi point, its topological nature can be transferred to the resultant insulating state, giving rise to intriguing phases such as spontaneous quantum Hall or quantum spin-Hall states [2].

The most famous Fermi point is the Dirac point. The Fermi “surface” of a half-filled honeycomb lattice, like graphene, consists of a pair of these points. Each Dirac point is similar to a vortex in the Brillouin zone (BZ) and is characterized by a topological winding number $n = \pm 1$ [1]. Haldane showed that the inclusion of complex hoppings in a honeycomb lattice opens up a gap at both Dirac points, giving rise to a quantum Hall state in absence of external magnetic field [3]. Similar ideas for realizing quantum Hall insulators through gapped Dirac points have been explored in double-exchange models on square, kagome, and checkerboard lattices [4–6]. By creating and manipulating Dirac points with the aid of artificial gauge fields, it is also possible to control topological phase transitions in optical lattices [7, 8].

Quantum Hall effect can also be induced by opening a gap at a topological Fermi point with a quadratic band dispersion [9]. These points are vortices carrying multiple topological charges $n = \pm 2$ in momentum space [10, 11]. Because of its higher winding numbers, a quadratic Fermi point can decay into several elementary Dirac points while preserving the total topological charge [10]. Unlike Dirac points where interaction effects are suppressed due to a vanishing density of states (DOS), quadratic Fermi points are unstable against arbitrarily weak short-range interactions due to their finite DOS [9, 12]. These Fermi points are usually protected in lattice models by C_4 or C_6 point group symmetries. Explicit examples are tight-binding models on checker-

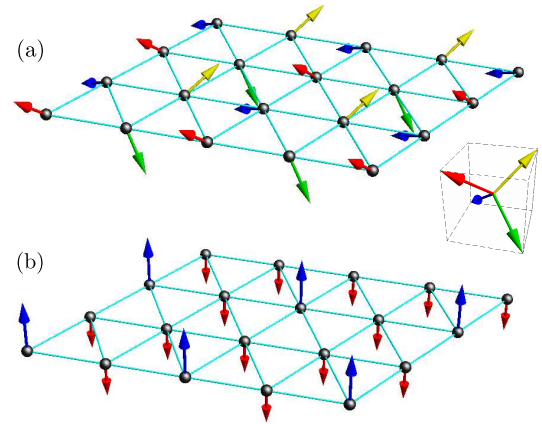


FIG. 1: (Color online) (a) Noncoplanar spin order with a quadrupled unit cell on a triangular lattice. The magnetic moments at the four sublattices point toward corners of a regular tetrahedron (see the inset). (b) Collinear spin order on the triangular lattice. In the enlarged unit cell, one site has large spin moment 3Δ while the other three sites have small moment $-\Delta$.

board and kagome lattices, respectively [9, 13]. Topological quadratic Fermi points also appear in physical systems such as bilayer graphene [14–19], photonic crystals [20], oxide heterostructures [21], and surface state of topological insulators [22].

In this paper we present the first example of a quadratic Fermi point with non-zero winding numbers that emerges from a topologically trivial Fermi surface through electron interactions. This special Fermi point results from a collinear triple- \mathbf{Q} magnetic ordering that is favoured by perfect nesting of the original Fermi surface. Moreover, by analyzing the stability of this emergent Fermi point, we demonstrate that a non-coplanar chiral spin order is always more stable than any other triple- \mathbf{Q} ordering (collinear or coplanar) as temperature tends to zero. The simple reason is that the non-coplanar state lowers its energy by opening a gap at the emergent Fermi point that also leads to *spontaneous quantum Hall effect*.

To illustrate these phenomena we consider Hubbard-like models on 2D lattices with a C_6 symmetry such as triangular or honeycomb lattices. It has been shown recently that the spin-density-wave (SDW) ground state of such models has a noncoplanar chiral order when the chemical potential reaches the saddle-point of the band structures [23–27]. This magnetic ordering has a quadrupled unit cell with local spins pointing toward corners of a regular tetrahedron; an example of such ordering on the triangular lattice is shown in Fig. 1(a).

The spontaneous quantum Hall effect of the SDW state arises from a non-zero scalar spin chirality $\langle \mathbf{S}_i \cdot \mathbf{S}_j \times \mathbf{S}_k \rangle$ of the underlying magnetic structure [23, 28]. When conduction electrons propagate through such a spin texture, their wavefunction acquires a Berry phase which is equal to half the solid angle subtended by local moments of each elementary plaquette. The Berry flux which is indistinguishable from a real magnetic flux induces the quantum Hall effect. Indeed, quantized Hall conductivity $\sigma_{xy} = e^2/h$ has been explicitly calculated for the chiral SDW state in both triangular and honeycomb lattices [23, 24, 26, 28].

Here we show that the recently discovered finite-temperature SDW phase with *collinear* magnetic moments [29] provides a useful starting point for understanding the origin of the spontaneous quantum Hall effect that necessarily appears at lower temperatures. A striking feature of this collinear SDW state shown in Fig. 1(b) is the existence of a quadratic Fermi point in its mean-field band structure [29]. Gapless charge excitations in this SDW state exist only for one spin branch. More importantly, we show that the quadratic Fermi point has a topological winding number $n = \pm 2$. We derive a universal low-energy Hamiltonian for excitations around the Fermi point. Remarkably, the gap of the quantum Hall state is proportional to the scalar spin chirality of the ordered spin state. Consequently, the transition from collinear to chiral SDW order coincides with the onset of quantum Hall effect.

We start by considering SDW instabilities in 2D lattices with a C_6 symmetry, such as triangular, honeycomb, kagome and their decorated variants [30]. The tight-binding DOS includes one or two Van Hove singularities. For example, a logarithmically divergent DOS appears for filling factor $3/4$ in the triangular lattice, and $3/8$ or $5/8$ in the honeycomb lattice. At these filling factors, the Fermi surface is a regular hexagon inscribed within the BZ; see Fig. 2(a). Remarkably, pairs of parallel edges of this Fermi surface are perfectly nested by wavevectors \mathbf{Q}_η which are equal to half of reciprocal lattice vectors. The perfect Fermi surface nesting is quite robust and is broken only by the inclusion of third nearest-neighbor or longer range hopping amplitudes.

SDW order appears as a weak-coupling instability induced by perfect Fermi surface nesting. In particular, the nature of the SDW instability is mainly controlled by

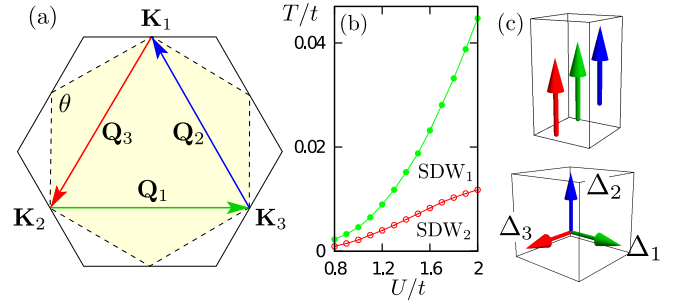


FIG. 2: (Color online) (a) The Brillouin zone of lattices with a C_6 symmetry and the Fermi surface when electron filling reaches the Van Hove singularity of the band structure. The three nesting wavevectors are $\mathbf{Q}_1 = (2\pi/\sqrt{3}, 0)$ and $\mathbf{Q}_{2,3} = (-\pi/\sqrt{3}, \pm\pi)$. (b) Phase diagram of the triangular-lattice Hubbard model. SDW₁ and SDW₂ denote spin-density-wave states with collinear and noncoplanar magnetic moments, respectively. (c) Configurations of the three vector order parameters Δ_η in the collinear (top) and chiral ‘tetrahedral’ (bottom) SDW phase.

the states that are close to the saddle points \mathbf{K}_η shown in Fig. 2(a) ($\eta = 1, 2, 3$), where a vanishing Fermi velocity gives rise to a logarithmically divergent DOS. The effective Hamiltonian for the SDW ordering expressed in terms of these low-energy electrons is [29]

$$\begin{aligned}
 H = & \sum_{\eta;\alpha;\mathbf{k}} \varepsilon_\eta(\mathbf{k}) c_{\eta\alpha,\mathbf{k}}^\dagger c_{\eta\alpha,\mathbf{k}} \\
 & - \sum_{\xi \neq \zeta; \alpha; \beta} \sum_{\mathbf{k}; \mathbf{q}; \mathbf{p}} g_{\alpha,\beta} c_{\xi\alpha,\mathbf{k}-\mathbf{q}}^\dagger c_{\xi\beta,\mathbf{k}+\mathbf{q}}^\dagger c_{\zeta\beta,\mathbf{k}+\mathbf{p}} c_{\zeta\alpha,\mathbf{k}-\mathbf{p}} \\
 & + \sum_{\xi \neq \zeta; \alpha; \beta} \sum_{\mathbf{k}; \mathbf{q}; \mathbf{p}} g'_{\alpha,\beta} c_{\xi\alpha,\mathbf{k}-\mathbf{q}}^\dagger c_{\zeta\beta,\mathbf{k}+\mathbf{q}}^\dagger c_{\zeta\beta,\mathbf{k}+\mathbf{p}} c_{\xi\alpha,\mathbf{k}-\mathbf{p}} ,
 \end{aligned} \tag{1}$$

where $c_{\eta\alpha,\mathbf{k}}^\dagger$ creates an electron with spin $\alpha = \uparrow, \downarrow$ and momentum $\mathbf{K}_\eta + \mathbf{k}$ ($|\mathbf{k}| \ll 1$), while g and g' denote the forward and umklapp scatterings, respectively [29]. The dispersion around the three saddle points is given by $\varepsilon_\eta(\mathbf{k}) = k_\xi k_\zeta / m^*$, where $1/m^* \sim \mathcal{O}(t)$ is of the order of bandwidth, $(\eta\xi\zeta)$ is a cyclic permutation of (123), and $k_\xi = \mathbf{k} \cdot \hat{\mathbf{e}}_\xi$, with $\hat{\mathbf{e}}_3 = (1, 0)$ and $\hat{\mathbf{e}}_{1,2} = (-\frac{1}{2}, \pm\frac{\sqrt{3}}{2})$. For the special case of Hubbard model, we have $g = g' = U\delta_{\alpha,\bar{\beta}}/N$, where U is the on-site Coulomb repulsion, $\bar{\beta}$ denotes the opposite spin, and N is the total number of sites. Although renormalization-group (RG) analysis indicated that superconductivity instability is asymptotically dominant [31], the SDW vertex is the largest at intermediate RG scale and becomes dominant by slightly doping away from the Van Hove singularity [32].

The effective filling fraction restricted to this low-energy model can be obtained by a simple geometrical consideration. As shown in Fig. 2(a), the filled region in the vicinity of a saddle point is bounded by two straight lines with an angle $\theta = 2\pi/3$ between them. This gives rise to an effective filling factor: $\nu_{\text{eff}} = \theta/\pi = 2/3$. In the

folded BZ of the triple- \mathbf{Q} SDW states, the three saddle points are shifted to the zone center; each corresponds to two electron bands with different spin species. An effective 2/3 filling indicates that 4 out of the 6 bands are filled in the insulating state.

The component of the SDW order parameter associated with the nesting wavevector \mathbf{Q}_η is $\Delta_\eta = \frac{v}{3} \sum_{\mathbf{k}} \langle c_{\xi\alpha,\mathbf{k}}^\dagger \sigma_{\alpha\beta} c_{\zeta\beta,\mathbf{k}} \rangle$, where $v = g + g'$. A mean-field decoupling of the interaction terms in (1) based on this SDW order parameter yields a Hamiltonian:

$$H_{\text{MF}} = \frac{1}{v} \int d\mathbf{r} \sum_{\eta} |\Delta_\eta|^2 + \sum_{\xi\zeta} \sum_{\alpha\beta,\mathbf{k}} c_{\xi\alpha,\mathbf{k}}^\dagger \mathcal{M}_{\xi\alpha,\zeta\beta} c_{\zeta\beta,\mathbf{k}}, \quad (2)$$

with the interaction matrix:

$$\mathcal{M}(\mathbf{k}) = \begin{pmatrix} k_2 k_3 \mathbb{I} & \Delta_3 \cdot \boldsymbol{\sigma} & \Delta_2 \cdot \boldsymbol{\sigma} \\ \Delta_3 \cdot \boldsymbol{\sigma} & k_3 k_1 \mathbb{I} & \Delta_1 \cdot \boldsymbol{\sigma} \\ \Delta_2 \cdot \boldsymbol{\sigma} & \Delta_1 \cdot \boldsymbol{\sigma} & k_1 k_2 \mathbb{I} \end{pmatrix}. \quad (3)$$

Here \mathbb{I} is a 2×2 identity matrix, $\boldsymbol{\sigma} = (\sigma^x, \sigma^y, \sigma^z)$ is a vector of Pauli matrices, and we have set $m^* = 1$ for simplicity.

To examine the structure of the SDW state near the ordering temperature, a Ginzburg-Landau expansion up to sixth order in Δ was derived in Ref. [29] by integrating out the fermions. The analysis found that a collinear SDW state with $\Delta_1 = \Delta_2 = \Delta_3$ is favored immediately below the magnetic transition; the corresponding spin order is shown in Fig. 1(b). At a lower temperature, the system undergoes another transition into a chiral SDW state whose three components of the order parameter are orthogonal to each other and have the same amplitude, as shown in Fig. 2(c). The real-space magnetic order shown in Fig. 1(a) has a quadrupled unit cell with local spins pointing toward different corners of a regular tetrahedron. An explicit calculation for the triangular-lattice Hubbard model gives a phase diagram shown in Fig. 2(b), which is consistent with the two-stage ordering scenario described above.

The collinear SDW state is a half-metal which hosts a Fermi point at the center of the folded BZ; its mean-field band structure is shown in Fig. 3(a). To understand the nature of this gapless point, we first focus on the fermion spectrum at $\mathbf{k} = 0$. We assume that the three order parameters have the same amplitude Δ , as such states are favoured by the fourth order contributions to the energy expansion in powers of Δ_η [29]. The interaction matrix (3) at the Γ point in *momentum* space is equivalent to a tight-binding problem on a triangular loop (see Fig. 3(c)) with a spin-dependent hopping $t_{ij} = t U_{ij} = \Delta_\eta \cdot \boldsymbol{\sigma} = \Delta \exp(i \frac{e}{h} \int \mathbf{A} \cdot d\mathbf{r})$, where \mathbf{A} is a non-Abelian gauge potential. Its spectrum depends only on the gauge-invariant Wilson loop $W = \text{tr}(U_{12} U_{23} U_{31})$. Interestingly, this non-Abelian flux is proportional to the scalar spin chirality

$$W = -i \Delta_1 \cdot (\Delta_2 \times \Delta_3) / \Delta^3. \quad (4)$$

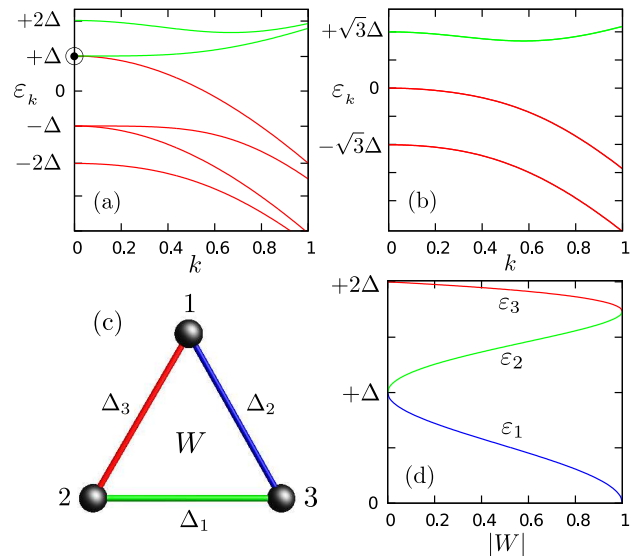


FIG. 3: (Color online) The mean-field band structure along $\mathbf{k} = (k, 0, 0)$ in the folded BZ for the (a) collinear and (b) noncoplanar SDW states. The calculation is done for the special case of triangular lattice. The quadratic Fermi point with winding number $n = \pm 2$ is marked by \odot in panel (a). Each band in the noncoplanar SDW state is doubly degenerate. (c) An equivalent tight-binding model on the triangular loop for Hamiltonian (3). (d) Energy levels at the $\mathbf{k} = 0$ as a function of the invariant Wilson loop W . The collinear and tetrahedral SDW states have $|W| = 0$ and 1, respectively.

Explicitly, the energy levels at the Γ point are solutions of the polynomial equation: $\varepsilon^2(\varepsilon^2 - 3)^2 + 4(|W| - 1) = 0$, and always appear in $\pm\varepsilon_m$ pairs. Fig. 3(d) shows the three positive eigen-energies as a function of the non-Abelian flux. Noting that there are three bands with negative energy, the charge gap at 2/3 filling is given by $\Delta\varepsilon = \varepsilon_2 - \varepsilon_1$. This gap closes only when $W = 0$, i.e. for any coplanar, and particularly collinear, SDW state.

We now show that the transition from collinear to chiral SDW states is a topological phase transition involving a quadratic Fermi point. Without loss of generality, we assume $\Delta_1 = \Delta_2 = \Delta_3 = \Delta \hat{z}$ for the collinear order. The low-energy electrons in the vicinity of the emergent Fermi point come from the two bands ε_1 and ε_2 in Fig. 3(d); the corresponding eigenstates are $\psi_1 = \frac{1}{\sqrt{2}}(c_{1\downarrow} - c_{2\downarrow})$ and $\psi_2 = \frac{1}{\sqrt{6}}(c_{1\downarrow} + c_{2\downarrow} - 2c_{3\downarrow})$, respectively. Introducing a pseudospin $\tau^z = \pm 1$ to label these two states, the low-energy Hamiltonian in this basis is given by

$$\mathcal{H}(\mathbf{k}) = h_0 \mathbb{I} + d_x \tau^x + d_z \tau^z, \quad (5)$$

where τ^x and τ^z are Pauli matrices and

$$\begin{aligned} h_0 &= \Delta - (k_x^2 + k_y^2)/4, \\ d_x &= k_x k_y / 2, \quad d_z = (k_x^2 - k_y^2)/4. \end{aligned} \quad (6)$$

A diagonalization of $\mathcal{H}(\mathbf{k})$ yields a flat band $\varepsilon_{1,\mathbf{k}} = \Delta$ and a quadratic band $\varepsilon_{2,\mathbf{k}} = \Delta - |\mathbf{k}|^2/2$. The pseudovector

field $\mathbf{d} = (d_x, d_z)$ shown in Fig. 4(b) has d -wave symmetry. The topological charge for the singular $\mathbf{k} = 0$ point is given by the winding number of pseudovector field: $n = \frac{1}{2\pi} \oint_{\mathcal{C}} \nabla \theta_d(\mathbf{k}) \cdot d\mathbf{k} = \pm 2$ [1], where $\theta_d = \arctan(d_z/d_x)$ and \mathcal{C} is a contour enclosing the Fermi point.

The existence of this topological Fermi point is protected by the C_6 symmetry preserved in the collinear SDW phase and the spin collinearity masqueraded as an effective time-reversal symmetry. Further symmetry-breaking at lower temperatures could remove the quadratic Fermi point by either splitting it into elementary Dirac points or simply opening a gap. To study the stability of the collinear SDW state, we introduce small deviations to the order parameters: $\Delta_\eta = \Delta \hat{\mathbf{z}} + \mathbf{m}_\eta$ with $\mathbf{m}_\eta \perp \hat{\mathbf{z}}$. Substituting into Eq. (2) and projecting to the low-energy doublet manifold $\Psi = (\psi_1, \psi_2)$, the mean-field Hamiltonian becomes

$$H_{\text{MF}} = \frac{1}{v'} \int d\mathbf{r} \sum_{\eta} |\mathbf{m}_\eta|^2 + \sum_{\mathbf{k}} \Psi_{\mathbf{k}}^\dagger \mathcal{H}(\mathbf{k}) \Psi_{\mathbf{k}} \quad (7)$$

$$+ \int d\mathbf{r} \Psi^\dagger(\mathbf{r}) \left[\frac{1}{\sqrt{6}\Delta} (\mathcal{Q}_1 \tau^z + \mathcal{Q}_2 \tau^x) + \frac{\kappa}{\sqrt{3}\Delta^2} \tau^y \right] \Psi(\mathbf{r}),$$

where $1/v' = 1/v + 1/6\Delta$ is the effective inverse coupling. The doublet order parameter $(\mathcal{Q}_1, \mathcal{Q}_2)$ given by

$$\begin{aligned} \mathcal{Q}_1 &= (|\mathbf{m}_1|^2 + |\mathbf{m}_2|^2 - 2|\mathbf{m}_3|^2)/\sqrt{6}, \\ \mathcal{Q}_2 &= (|\mathbf{m}_1|^2 - |\mathbf{m}_2|^2)/\sqrt{2}, \end{aligned} \quad (8)$$

describes a nematic phase for the Ψ fermions in which the C_6 rotational symmetry is broken down to C_2 by splitting the quadratic Fermi point into two Dirac points. The corresponding SDW order is dominated by a single nesting wavevector. The nematic phase remains a half-metal. Since the total winding number is conserved, the two residual Dirac points in the nematic phase carry the same topological charges. The order parameter κ is the scalar spin chirality (4):

$$\begin{aligned} \kappa &= \Delta_1 \cdot (\Delta_2 \times \Delta_3) = \Delta (m_1^x m_2^y - m_1^y m_2^x \\ &\quad + m_2^x m_3^y - m_2^y m_3^x + m_3^x m_1^y - m_3^y m_1^x). \end{aligned} \quad (9)$$

It characterizes an insulating phase with broken time-reversal symmetry and a zero-field quantized Hall conductivity $\sigma_{xy} = e^2/h$.

Minimization of Eq. (7) yields a ground state that preserves the C_6 rotational symmetry while breaking the effective time-reversal symmetry. The transition from the $\kappa = 0$ phase into the quantum Hall state with $\kappa \neq 0$ is a discontinuous one. To see this, we compute the ground-state energy of (7) as a function of κ [33]:

$$\frac{E(\kappa)}{V} = \frac{2|\kappa|}{\sqrt{3}v'\Delta} - \frac{\rho^* \kappa^2}{6\Delta^4} \log \frac{\Lambda}{|\kappa|}, \quad (10)$$

where ρ^* is the density of states at the quadratic Fermi point, Λ is an ultraviolet cutoff, and V is the system

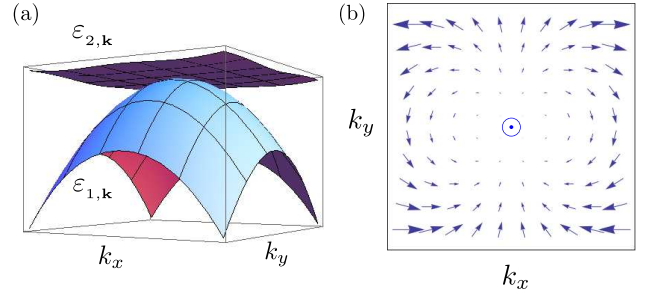


FIG. 4: (Color online) (a) Fermi point at a quadratic band crossing at $\mathbf{k} = 0$. (b) The pseudovector field $\mathbf{d} = (d_x, d_z)$ with $d_x = (k_x^2 - k_y^2)/4$ and $d_z = k_x k_y/2$ resembles a vortex in XY systems with a winding number $n = 2$.

volume. The function $E(\kappa)$ has two minima at $\kappa = 0$ and $\kappa \sim \Lambda/\sqrt{e}$. At higher temperatures, the system may remain in the $\kappa = 0$ minimum corresponding to the collinear SDW state, as it was found in Ref. [29] for a Hubbard model on triangular and honeycomb lattices. Upon lowering the temperature, the system switches to the absolute minimum with $\kappa = \pm\Delta^3$ (since the triple product is bounded) which corresponds to the non-coplanar tetrahedral order.

The first-order transition scenario is consistent with our explicit mean-field calculations of the Hubbard model on triangular or honeycomb lattices. It is worth noting that the collinear SDW phase is stabilized by thermal fluctuations at finite temperatures. A lower free energy of the uniaxial SDW state results from the gapless electronic excitations and the softer magnetic fluctuations associated with collinear spin order. Although the collinear SDW state hosting a topological Fermi point has been shown to exist in three of the most representative 2D lattices with C_6 rotational symmetry [29, 33], and maybe also in their decorated variants, its stability at finite temperatures depends on details of the model.

To summarize, we have shown the emergence of a quadratic Fermi point characterized by a winding number $n = \pm 2$ in triple- \mathbf{Q} collinear SDW states of different two-dimensional lattices. Such SDW phase arises from a perfectly nested Fermi surface in lattices with a six-fold rotational symmetry such as triangular, honeycomb, or kagome. Unlike most topological Fermi points which result from the special band structures of certain lattice problems, this quadratic Fermi point emerges from a topologically trivial Fermi surface through electron interactions. We have also obtained a universal low-energy Hamiltonian for the quadratic Fermi point and showed that the instability towards a quantum Hall insulator is described by an order parameter which corresponds to the scalar spin chirality. Our theory thus explains why the topologically non-trivial (non-coplanar) SDW order is always more stable than the topologically trivial coplanar states at low temperatures.

Although spontaneous quantum Hall effect has been extensively discussed in the context of double-exchange or Kondo-lattice models, most of these studies assume classical localized moments to begin with. It is then natural to ask if this phenomenon survives for models that incorporate quantum spin fluctuations. Our analysis of the noncoplanar SDW ordering in Hubbard-like models provides a positive answer to this important question. Possible material realizations of the collinear SDW phase that hosts the topological Fermi point include triangular compound $\text{Na}_{0.5}\text{CoO}_2$ [34] and doped graphene [35].

Acknowledgement. We thank A. Chubukov, R. Fernandez, Y. Kato, I. Martin, and R. Nandkishore for useful discussions. Work at LANL was carried out under the auspices of the U.S. DOE contract No. DE-AC52-06NA25396 through the LDRD program. G.W.C. is grateful to the hospitality of CNLS at LANL and the support of ICAM and NSF grant DMR-0844115.

-
- [1] G. E. Volovik, *The Universe in a Helium Droplet* (Clarendon, Oxford, 2003).
- [2] M. Z. Hasan and C. L. Kane, *Rev. Mod. Phys.* **82**, 3045 (2010); X.-L. Qi and S.-C. Zhang, *ibid.* **83**, 1057 (2011).
- [3] F. D. M. Haldane, *Phys. Rev. Lett.* **61**, 2015 (1988).
- [4] X. Chen, S. Dong, and J.-M. Liu, *Phys. Rev. B* **81**, 064420 (2010).
- [5] K. Ohgushi, S. Murakami, and N. Nagaosa, *Phys. Rev. B* **62**, R6065 (2000).
- [6] J. W. F. Venderbos, M. Daghofer, J. van den Brink, and S. Kumar, arXiv:1202.3340.
- [7] N. Goldman, A. Kubasiak, A. Bermudez, P. Gaspard, M. Lewenstein, and M. A. Martin-Delgado, *Phys. Rev. Lett.* **103**, 035301 (2009).
- [8] A. Bermudez, N. Goldman, A. Kubasiak, M. Lewenstein, and M. A. Martin-Delgado, *New J. Phys.* **12**, 033041 (2010).
- [9] K. Sun, H. Yao, E. Fradkin, and S. Kivelson, *Phys. Rev. Lett.* **103**, 046811 (2009).
- [10] T. T. Heikkilä and G. E. Volovik, *JETP Lett.* **92**, 681 (2010).
- [11] Quadratic Fermi point with zero winding number is an accidental band crossing and can be removed by small perturbations without breaking any symmetries.
- [12] S. Uebelacker and C. Honerkamp, *Phys. Rev. B* **84**, 205122 (2011).
- [13] Q. Liu, H. Yao, and T. Ma, *Phys. Rev. B* **82**, 045102 (2010); An example in the Lieb lattice is discussed in W.-F. Tsai, C. Fang, H. Yao, J. Hu, arXiv:1112.5789.
- [14] J. L. Mañes, F. Guinea, and M. A. H. Vozmediano, *Phys. Rev. B* **75**, 155424 (2007).
- [15] P. Dietl, F. Piechon, and G. Montambaux, *Phys. Rev. Lett.* **100**, 236405 (2008).
- [16] H. Min, G. Borghi, M. Polini, and A. H. MacDonald, *Phys. Rev. B* **77**, 041407(R) (2008).
- [17] I. Martin, Ya. M. Blanter, and A. F. Morpurgo, *Phys. Rev. Lett.* **100**, 036804 (2008).
- [18] O. Vafek and K. Yang, *Phys. Rev. B* **81**, 041401 (2010).
- [19] R. Nandkishore and L. Levitov, *Phys. Rev. Lett.* **104**, 156803 (2010).
- [20] Y. D. Chong, X.-G. Wen, and M. Soljacic, *Phys. Rev. B* **77**, 235125 (2008).
- [21] S. Banerjee, R. R. P. Singh, V. Pardo, and W. E. Pickett, *Phys. Rev. Lett.* **103**, 016402 (2009).
- [22] L. Fu, *Phys. Rev. Lett.* **106**, 106802 (2011).
- [23] I. Martin and C. D. Batista, *Phys. Rev. Lett.* **101**, 156402 (2008).
- [24] T. Li, arXiv:1001.0620 (2010).
- [25] W.-S. Wang, Y.-Y. Xiang, Q.-H. Wang, F. Wang, F. Yang, and D.-H. Lee, *Phys. Rev. B* **85**, 035414 (2012).
- [26] T. Li, arXiv:1103.2420 (2011).
- [27] S.-L. Yu and J.-X. Li, *Phys. Rev. B* **85**, 144402 (2012).
- [28] R. Shindou and N. Nagaosa, *Phys. Rev. Lett.* **87**, 116801 (2001).
- [29] R. Nandkishore, G.-W. Chern, and A. V. Chubukov, *Phys. Rev. Lett.* **108**, 227204 (2012).
- [30] A. Rüegg, J. Wen, and G. A. Fiete, *Phys. Rev. B* **81**, 205115 (2010).
- [31] R. Nandkishore, L. S. Levitov and A. V. Chubukov, *Nature Phys.* **8**, 158 (2012).
- [32] M. Kiesel, C. Platt, W. Hanke, D. A. Abanin, R. Thomale, arXiv:1109.2953v1.
- [33] See supplementary material for the triple-**Q** collinear SDW on Kagome and discussion on the ground-state energy.
- [34] F. L. Ning, S. M. Golin, K. Ahilan, T. Imai, G. J. Shu, and F. C. Chou, *Phys. Rev. Lett.* **100**, 086405 (2008).
- [35] J. L. McChesney, A. Bostwick, T. Ohta, T. Seyller, K. Horn, J. González, and E. Rotenberg, *Phys. Rev. Lett.* **104**, 136803 (2010).

SUPPLEMENTARY MATERIALS

KAGOME LATTICE

The triple- \mathbf{Q} spin-density-wave (SDW) states in triangular and honeycomb lattices have been discussed in Refs. [1–3]. Here we consider another representative two-

$$\begin{aligned}\mathbf{S}_\alpha(\mathbf{r}) &= +\Delta_1 \cos(\mathbf{Q}_1 \cdot \mathbf{r}) + \Delta_2 \cos(\mathbf{Q}_2 \cdot \mathbf{r}) + \Delta_3 \cos(\mathbf{Q}_3 \cdot \mathbf{r}), \\ \mathbf{S}_\beta(\mathbf{r}) &= +\Delta_1 \cos(\mathbf{Q}_1 \cdot \mathbf{r}) - \Delta_2 \cos(\mathbf{Q}_2 \cdot \mathbf{r}) - \Delta_3 \cos(\mathbf{Q}_3 \cdot \mathbf{r}), \\ \mathbf{S}_\gamma(\mathbf{r}) &= -\Delta_1 \cos(\mathbf{Q}_1 \cdot \mathbf{r}) - \Delta_2 \cos(\mathbf{Q}_2 \cdot \mathbf{r}) + \Delta_3 \cos(\mathbf{Q}_3 \cdot \mathbf{r}),\end{aligned}\tag{11}$$

where α , β , and γ denote the three sublattices, and vector order parameters $\Delta_{1,2,3}$ have the same amplitude and are orthogonal to each other. Since the unit cell of kagome lattice contains three inequivalent sites, there are several triple- \mathbf{Q} collinear SDW orderings with different arrangements of spins within the unit cell. The collinear SDW state that is topologically connected to the tetrahedral order is obtained from Eq. (1) above by continuously closing the solid angle between the three vector order parameters Δ_i . By setting $\Delta_1 = \Delta_2 = \Delta_3 = \Delta \hat{\mathbf{z}}$, the resulting collinear SDW state is shown in Fig. 5(b) in which 3 sites in the quadrupled unit cell have magnetic moment 3Δ while the moment at the remaining 9 sites is $-\Delta$.

We now consider the Kondo-lattice model, which can be viewed as the mean-field approximation of the Hubbard-like model, on the kagome lattice:

$$H = -t \sum_{\langle ij \rangle} c_{i,\alpha}^\dagger c_{j,\alpha} - J_H \sum_i \mathbf{S}_i \cdot c_{i,\alpha}^\dagger \boldsymbol{\sigma}_{\alpha\beta} c_{j,\beta}. \tag{12}$$

where $\mathbf{S}_i = \frac{1}{2} \langle c_{i,\alpha}^\dagger \boldsymbol{\sigma}_{\alpha\beta} c_{j,\beta} \rangle$ is the local magnetic moment. The band structure of the nearest-neighbor tight-binding model ($J_H = 0$) is shown in Fig. 6(a). A logarithmically divergent density of states occurs at 1/4-filling due to perfectly nested Fermi surface. Figs. 6(b) and (c) shows the mean-field band structures in the presence of collinear and tetrahedral SDW order, respectively. At 1/4-filling, the lowest 6 bands are completely filled, giving rise to a quadratic Fermi point at $\mathbf{k} = 0$ (Γ point in the folded Brillouin zone) [Fig. 6(b)]. On the other hand, the non-coplanar tetrahedral order opens a charge gap as shown in Fig. 6(c).

With the addition of the kagome case discussed here, we have demonstrated the existence of triple- \mathbf{Q} collinear SDW state and its topological connection to the non-coplanar SDW order in three of the most representative 2D lattices with C_6 symmetry, namely triangular, hon-

dimensional lattice with C_6 rotational symmetry: the case of kagome lattice. The existence and stability of non-coplanar tetrahedral SDW order on kagome lattice, shown in Fig. 5(a), has been demonstrated in Ref. [4]. The non-coplanar tetrahedral order shown in Fig. 5(a) can be described as

eycomb, and kagome lattices. Although perfect Fermi surface nesting and divergent Van Hove singularities also exist in other lattices such as the decorated variants of the above three lattices, the properties of the triple- \mathbf{Q} SDW ordering will be left for future studies.

GROUND-STATE ENERGY

In this section we discuss the derivation of ground state energy Eq. (10) in the main text.

$$\frac{E(\kappa)}{V} = \frac{2|\kappa|}{\sqrt{3}v'\Delta} - \frac{\rho^* \kappa^2}{6\Delta^4} \log \frac{\Lambda}{|\kappa|}, \tag{13}$$

The first term is the energy cost when spins deviate from the collinear limit. It comes from the term $\frac{1}{v'} \sum_\eta |\mathbf{m}_\eta|^2$ in the effective Hamiltonian Eq. (7) of the main text. As also discussed there, the ground state preserves the C_6 rotational symmetry, hence the nematic order parameter vanishes $\mathcal{Q}_1 = \mathcal{Q}_2 = 0$. The scalar spin chirality is then maximized when the three \mathbf{m}_η vectors lie in the same plane perpendicular to $\hat{\mathbf{z}}$ and point at 120° to one another. This gives rise to $\sum_\eta |\mathbf{m}_\eta|^2 = 2|\kappa|/\sqrt{3}\Delta$.

The presence of spin chirality κ opens a gap at the Fermi point. The dispersion of the two electron bands near the Γ point is: $\epsilon_{1,2}(\mathbf{k}) \approx h_0(\mathbf{k}) \pm \sqrt{|\mathbf{k}|^4 + \delta^2}$, where the energy gap $\delta = |\kappa|/\sqrt{3}\Delta^2$. Standard calculation gives an energy gain $\int d^2\mathbf{k} (\sqrt{|\mathbf{k}|^4 + \delta^2} - |\mathbf{k}|^2) \sim \kappa^2 \log(\Lambda/|\kappa|)$ which is logarithmically divergent with κ . Here Λ denotes an ultraviolet cutoff. This accounts for the second term in Eq. (3).

Fig. 7 shows the ground state energy $E(\kappa)$ as a function of the scalar chirality κ for a generic case. The first term in Eq. (3) which is linear in $|\kappa|$ gives rise to a local minimum at $\kappa = 0$, corresponding to the collinear SDW state. The function $E(\kappa)$ has a global minimum at $\kappa \sim \Lambda/\sqrt{e}$ coming from the second term in Eq. (3). However, since the scalar chirality is bounded $|\kappa| \leq \Delta^3$,

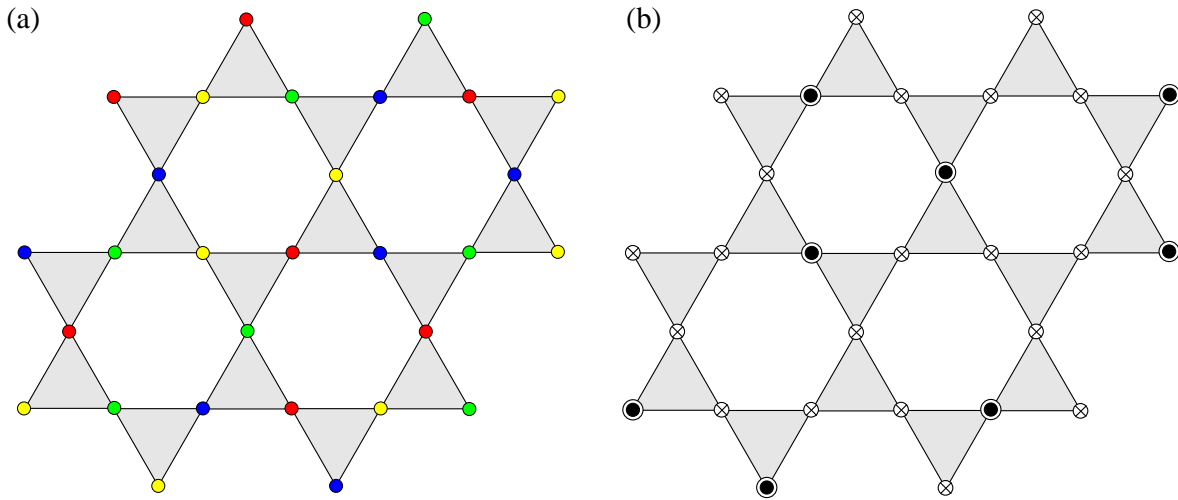


FIG. 5: (Color online) (a) The non-coplanar arrangement of local moments $\mathbf{S}(\mathbf{r})$ on the kagome lattice. Different colors correspond to the four non-coplanar spin directions pointing toward the corners of a regular tetrahedron. (b) The collinear triple- \mathbf{Q} SDW state on kagome. The local moments at the \odot and \otimes sites are 3Δ and $-\Delta$, respectively. The quadrupled unit cell in both SDW states contains 12 sites.

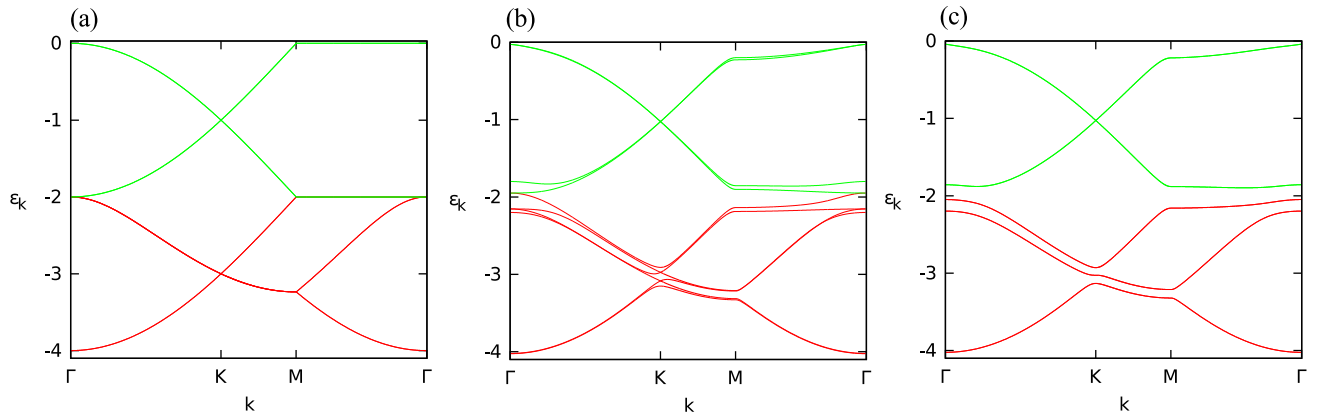


FIG. 6: (Color online) (a) Tight-binding band structure of kagome lattice shown with the folded Brillouin zone. (b) and (c) are the mean-field band structures of kagome Hubbard model in the presence of collinear and non-coplanar (tetrahedral) SDW ordering, respectively. At filling fraction $\nu = 1/4$, there exists a quadratic Fermi point at the Γ point in the collinear SDW state, while the spectrum is gapped in the non-coplanar SDW state.

the ground state is reached when the three order parameters Δ_η are perpendicular to each other, corresponding to the non-coplanar tetrahedral SDW order.

[2] T. Li, arXiv:1103.2420 (2011).

[3] R. Nandkishore, G.-W. Chern, and A. V. Chubukov, Phys. Rev. Lett. **108**, 227204 (2012).

[4] S.-L. Yu and J.-X. Li, Phys. Rev. B **85**, 144402 (2012).

[1] I. Martin and C. D. Batista, Phys. Rev. Lett. **101**, 156402 (2008).

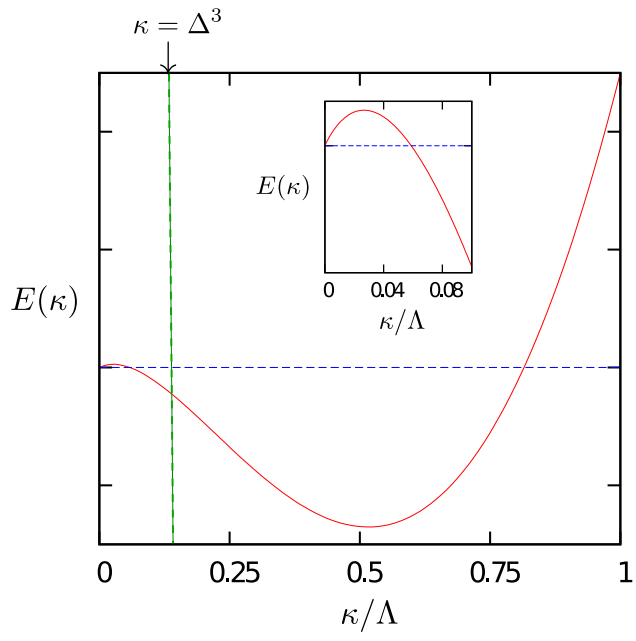


FIG. 7: (Color online) Ground-state energy $E(\kappa)$ as a function of the spin scalar chirality $\kappa = \mathbf{\Delta}_1 \cdot (\mathbf{\Delta}_2 \times \mathbf{\Delta}_3)$.